Formalism for the sequential estimation of neural membrane time constant and input–output curve towards selective and closed-loop transcranial magnetic stimulation*

S.M.Mahdi Alavi[a,*], Fidel Vila-Rodriguez[b], Adam Mahdi[c], Stefan M. Goetz[d,e]

[a]*Department of Applied Computing and Engineering, School of Technologies, Cardiff Metropolitan University, Cardiff, CF5 2YB, UK*
[b]*Department of Psychiatry, Faculty of Medicine, University of British Columbia, Vancouver, V6T 2A1, BC, Canada*
[c]*Oxford Internet Institute, University of Oxford, Oxford, OX1 3JS, UK*
[d]*Departments of Psychiatry & Behavioral Sciences, Electrical & Computer Engineering, and Neurosurgery, Duke University, Durham, 27708, NC, USA*
[e]*Department of Engineering, School of Technology, University of Cambridge, Cambridge, CB2 1PZ, UK*

Abstract

This paper describes a novel tool for closed-loop system identification of the activation dynamics of the neural target of transcranial magnetic stimulation (TMS). The method operates in real time, selects ideal stimulus parameters, detects and processes the response, and estimates the input–output (IO) curve and the neural membrane time constant representing a first-order approximation of the activated neural target. First, the neural membrane response and depolarization factor, which leads to motor evoked potentials (MEPs) are analytically computed and discussed. Then, an integrated model is developed which combines the neural membrane time constant and the input–output curve in TMS. Identifiability of the proposed integrated model is discussed. A condition is derived, which assures SPE of the proposed integrated model. Finally, a real-time and sequential parameter estimation (SPE) formalism is described to identify the neural membrane time constant and IO curve parameters in closed-loop TMS, where TMS pulses are administered sequentially based on the automatic analysis of the electromyography (EMG) data in real time. Optimal sampling based on maximization of the Fisher information matrix (FIM) and more conventional and intuitive uniform sampling methods both are addressed in this paper. The effectiveness of the proposed parameter tuning method is evaluated via simulations. Without loss of generality, this paper focuses on a specific case of cTMS pulses. The method is directly applicable to other cTMS pulse shapes with no new point of principals. The Matlab code is available online on Github.

Keywords: Transcranial magnetic stimulation (TMS), input–output (IO) curve, Neural membrane time constant, sequential parameter estimation, closed-loop system.

1. Introduction

Brain stimulation techniques, such as transcranial magnetic stimulation (TMS) or electrical stimulation (ES), can evoke neural signals through strong pulses and practically write signals into neurons in the brain, which the brain with its circuits can process similar to endogenous signals [1, 2, 3]. Medical use in therapy and diagnosis but also experimental brain research desire a high level of stimulation selectivity to target only specific groups of neurons. Whereas previously stimulation selectivity was mostly achieved through improving coil focality, limits have been reached [4] and temporal aspects of pulses to exploit the neuronal activation dynamics for a further improvement of stimulation selectivity have gained attention [5, 6]. Selective neural stimulation aims to target distinct neuronal populations based on the biophysical properties of axonal membrane [7, 8]. However, the activation dynamics of neurons can also serve for other techniques, such as detection of the actually activated neurons.

The activation dynamics are nonlinear and vary between neurons. However, typically the neural activation dynamics have a strong low-pass component, which can to some extent be approximated by a linear filter with a certain low-pass time constant. The neural membrane time constant, defined as the amount of time it takes for the linearized membrane depolarization to reach 63.2% of its final value in response to a step excitation [9], is one of the properties that significantly changes in various neurodegenerative disorders and therapeutic interventions. Its value depends on the axonal microanatomy, such as membrane resistance and capacitance, as well as the dynamics of the expressed ion channels and their sub-units [7, 10, 11].

Beyond basic neuroscientific research, the identification of the activation dynamics also has a substantial med-

*Matlab Code is available at https://github.com/smmalavi/TMS-tau-IOC-estim-fixed-tp

*Corresponding Author

[1]E-mails: malavi@cardiffmet.ac.uk, fidel.vilarodriguez@ubc.ca, adam.mahdi@oii.ox.ac.uk, smg84@cam.ac.uk

ical value. Neurophysiological studies confirm that the time constant decreases with hyperpolarization and it increases with depolarization, [12]. Thus, significant attempts have been made to develop time constant-based biomarkers for the characterization of the excitability of central and peripheral nerve systems. As an examples for recent achievements, studies demonstrated that the time constant increases with demyelination and is significantly longer than in healthy controls in neurodegenerative disorders such as amyotrophic lateral sclerosis (ALS) and severe spinal muscular atrophy [13, 14, 15]. After the intravenous immunoglobulin (IVIg) therapy, significant reduction of the time constant in chronic inflammatory demyelinating polyneuropathy (CIDP) [16]. Sensory fibers represent significantly longer time constant than motor fibers in healthy controls and patients with alcoholic polyneuropathy, [17].

The identification of the activation dynamics through measurement of the time constant of the activated neural elements is typically performed in targets with readily detectable response, such as the primary motor cortex or rarer the visual cortex [18]. In the primary motor cortex, strong stimulation pulses lead to visible muscle contraction in the periphery and weaker ones can be detected as motor evoked potentials (MEP), with latest methods even below the noise floor of background activity in electromyographic (EMG) recordings [19, 20, 21, 22].

The neural membrane time constant is usually measured through the strength–duration (S–D) curve, thus, it is also so-called the S–D time constant in some literature [12, 24, 25]. Each point on the S–D curve implies the pulse amplitude and duration required for threshold stimulation. The S–D curve is obtained by changing the pulse duration and titrating the stimulation threshold or a similarly stable level for each pulse duration. The time constant or sometimes the so-called chronaxie, which is loosely connected to the time constant, are often estimated by fitting the Lapicque model

$$I = \frac{I_r}{1 - e^{-t/\tau}}, \tag{1}$$

to the S–D curve, where I is the threshold current, t is time, I_r is the rheobase amplitude, and τ is the time constant [26]. The rheobase implies the minimum pulse amplitude required for threshold stimulation for an infinitely long-duration stimulus pulse. The pulse duration which requires twice rheobase for the threshold stimulation, is so-called the chronaxie, c, which is given in terms of the time constant as follows:

$$c \approx 0.7\tau. \tag{2}$$

Instead of (1), there is also a suggestion to estimate the S–D curve parameters and the time constant by using the Weiss model

$$I = I_r\Big(1 + \frac{c}{t}\Big), \tag{3}$$

which can result in a better fit [26].

In all these methods, the time constant is estimated offline, by using the S–D curve, which requires stimulations at various pulse widths and computation of the motor thresholds. Thus, a method which could estimate the time constant in real-time is demanding.

In [24], a model was developed based on the depolarization factor, which combines the neural membrane time constant and input–output (IO) curve in TMS. However, the depolarization factor was not computed analytically.

In this paper, the proposed integrated model is completed and discussed by analytical computation of the depolarization factor. Without loss of generality, the exact model of the controllable TMS (cTMS) pulses [8] with adjustable amplitude and width is addressed. Then, real-time sequential parameter estimation (SPE) of the neural membrane time constant and IO curve parameters is developed for both open-loop and closed-loop EMG-guided TMS.

Closed-loop TMS refers to the automatic and real-time adjustment of TMS parameters to maximize the desired plastic effects by using the brain/neural data in a feedback system [27, 28]. Closed-loop TMS is an area of active research using both closed-loop EEG-guided TMS [28, 29, 30, 31, 32] and closed-loop electromyography-guided (EMG-guided) TMS [33, 34].

In [33] and [34], two Fisher-information-based sequential parameter estimation (FIM SPE) methods have been developed for optimal IO curve and slope curve estimation in EMG-guided TMS. In the FIM SPE method, TMS pulse amplitudes are chosen automatically and sequentially based on prior responses in order to maximize the extracted information about the IO parameters. Thus, the FIM SPE is a closed-loop tuning method, which results in more accurate estimation of the IO curve and parameters with fewer numbers of TMS pulses, reducing the duration and discomfort of the procedure, compared to the uniform sampling method. In the uniform sampling IO curve estimation, which is an open-loop tuning method, the TMS stimuli are uniformly distributed between the minimum and maximum values, [35, 36, 37]. Despite simplicity, the uniform sampling method suffers from other drawbacks. For instance, it does not provide any information about the number of TMS pulses and their repetition. It is also not optimal in the sense that many TMS pulses might be administered that do not necessarily improve the IO curve estimation performance.

This paper develops an SPE of the neural membrane time constant and IO curve parameters based on optimal and uniform sampling methods. The effectiveness of the proposed parameter tuning method is evaluated via simulations in a detailed MEP model.

The contributions of this paper are then highlighted as follows:

- Analytical formalism for the estimation of the neural membrane response to cTMS pulses.
- Developing an analytical integrated model of the neu-

ral membrane time constant and IO curve parameters.

- Identifiability analysis of the proposed integrated model.
- Concurrent estimation of the neural membrane time constant and IO curve parameters for both open-loop and closed-loop TMS by using optimal and uniform sampling methods.

2. The integrated model

This section develops an integrated model of the neural membrane time constant and input–output (IO) curve.

2.1. The TMS pulse model

In all TMS devices, an electric pulse passes through the coil, which generates a time-varying magnetic field [38]. Without loss of generality, consider the specific electric pulse waveform $w(t)$ in a cTMS as shown in Fig. 1, which is a piece-wise signal given by [8, 39]

$$w(t) = \begin{cases} \delta \frac{V_C}{L}\left(\cos\omega t - \frac{\sigma}{\omega}\sin\omega t\right)e^{-\sigma t} & \text{if } t \le t_p, \\ -\delta \frac{V_C(R+r)\sin\omega t_p}{\omega L^2} e^{-\frac{(t-t_p)(R+r)}{L} - \sigma t_p} & \text{if } t > t_p, \end{cases} \tag{4}$$

where, V_C denotes the normalized pulse amplitude, based on the voltage of the capacitive energy storage C. It is assumed that V_C is adjustable between $V_C(\min) = 0$ and $V_C(\max) = 1$. t_p is the pulse width, which is assumed to be adjustable between $t_p(\min) = 10$ µs and $t_p(\max) = 200$ µs. Other parameters include the stimulating coil L, the energy dissipation resistor R, the resistor r which represents the combined resistance of the capacitor, inductor and semi-conductor switch. The parameters ω and σ are defined as

$$\omega = \sqrt{\frac{1}{LC} - \left(\frac{r}{2L}\right)^2}, \text{ and} \tag{5}$$

$$\sigma = \frac{r}{2L}. \tag{6}$$

The parameter δ is a proportionality coefficient which describes the coupling and depends on the number of turns as well as the geometry of the coil, and the electric conductivity profile of the brain [40].

Following the original cTMS design and without loss of generality, the following parameter values are used in this paper [8]: $L = 16$ µH, $C = 716$ µF, $R = 0.1\ \Omega$, $r = 20$ mΩ, $\delta = 3.2 \times 10^{-6}$ (V/m)(A/s).

Remark 1. *In conventional TMS devices, the pulse width is fixed [41, 38]. Thus, the proposed modeling is also applicable to them as a special case just as it is to more advanced TMS technology with more flexible pulse control [42, 43, 44].*

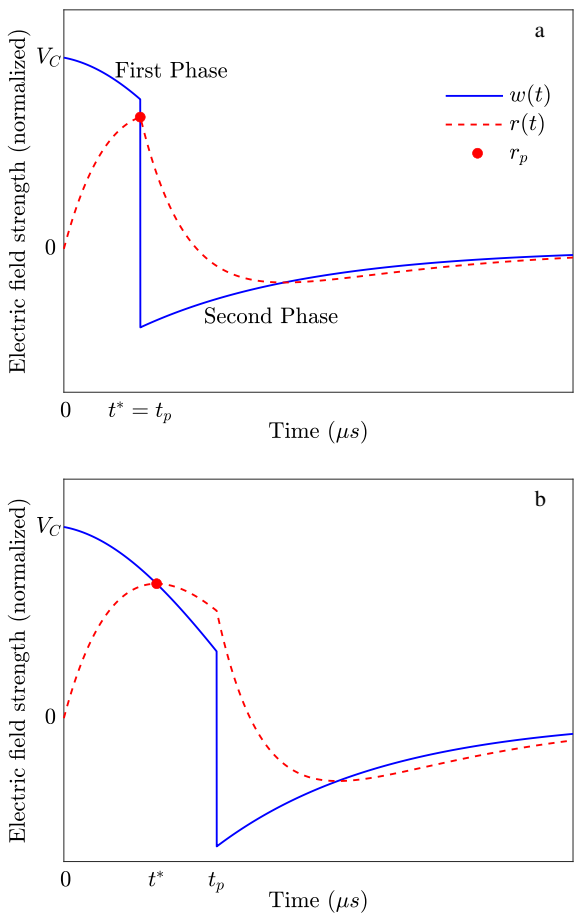

Figure 1: Two sample cTMS pulse waveforms with different pulse widths, and their responses of a neural membrane with the time constant τ. The depolarization factor r_p denotes the maximum (or peak) of $r(t)$, happening at $t = t^*$. a) A cTMS pulse, which results in r_p happening at $t^* = t_p$. b) By increasing the pulse width, r_p occurs at $t^* < t_p$.

2.2. The neural membrane model and response

The neural membrane depolarization response $r(t)$ is computed by the convolution of the administered pulse $w(t)$ and the neural membrane dynamic represented by its impulse response $h(t)$, which is approximated by a low-pass filter with time constant τ as follows [24, 45, 41]

$$h(t) = \frac{g_c}{\tau} e^{-t/\tau}. \tag{7}$$

Different first-order time constants have been reported in the literature, e.g. 196 µs in [24], (152 ± 26) µs in [45], and even more than 200 µs in [25]. This emphasizes the need for a method for the estimation of τ. The aim of this paper is to present a method for the sequential estimation of τ. The parameter g_c represents the coil-to-neuron coupling gain, which depends on factors such as the coil-to-cortex distance, head size, and neural population type and orientation relative to the induced electric field. The estimation of g_c is beyond the scope of this paper, and without loss of generality, we study the case of $g_c = 1$ in this paper.

Given $w(t)$ and $h(t)$, the neural membrane depolarization response $r(t)$ is obtained as

$$r(t) = \begin{cases} \frac{k_1 V_C}{\alpha\tau^2 - 2\sigma\tau + 1}\Big[-\omega e^{-t/\tau} + \\ \quad \Big((\alpha\tau - \sigma)\sin\omega t + \omega\cos\omega t\Big)e^{-\sigma t}\Big] & \text{if } t \le t_p, \\ r(t_p)e^{-(t-t_p)/\tau} + e^{-\sigma t_p}\Big(e^{-(t-t_p)/\tau} \\ \quad -e^{-(t-t_p)(R+r)/L}\Big)k_2 V_C & \text{if } t > t_p, \end{cases} \tag{8}$$

where, $r(t_p)$ is the neural membrane response at $t = t_p$, and

$$\alpha = \omega^2 + \sigma^2,$$
$$k_1 = \frac{g_c \delta}{L\omega},$$
$$k_2 = \frac{k_1(R+r)\sin\omega t_p}{\tau L(1/\tau - (R+r)/L)}.$$

Details of the formalism are given in Appendix A.

The depolarization factor r_p denotes the maximum or peak point of $r(t)$ defined as

$$r_p = r(t^*) = \max_{t=t^*} r(t), \tag{9}$$

where, t^* is the peak time.

Fig. 1 shows two cTMS pulse waveforms with different pulse widths, and their corresponding responses of a first-order neural membrane approximation with the time constant τ. It is observed that the maximum or peak point r_p occurs either at the end of the pulse ($t^* = t_p$) or before the end of the pulse ($t^* < t_p$).

The critical pulse width t_p^* is defined as the pulse width for which r_p occurs at $t^* = t_p$ for all pulse widths shorter than that, and r_p occurs at $t^* < t_p$ for all pulse widths longer than that. The values of t^* and t_p^* depend on the the pulse parameters and τ.

Fig. 2 shows the relationship between t_p^* and τ for the cTMS pulse parameters given in Section 2.1. It is seen that the critical pulse width increases exponentially with the membrane time constant. The next section discusses the importance of the critical pulse width on identifiability of the membrane time constant.

2.3. The input–output curve model

As shown in the literature, the IO curve, characterizing the relationships between the MEPs and pulse amplitudes would be sigmoidal for a fixed t_p when TMS pulses are administered with the same pulse-width t_p [24, 33, 46]. On the other hand, an MEP is generated when the depolarization factor r_p reaches a threshold.

Whereas earlier studies used to describe MEPs and IO curves linearly, research has demonstrated that IO curves reside in the log domain and show intricate variability characteristics [46, 47]. The variability can be normalized by log-transformation in the first approximation [48, 49].

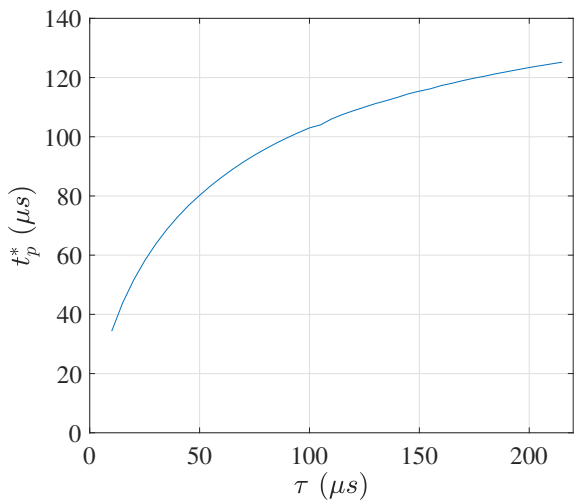

Figure 2: The relationship between the critical pulse width t_p^* and the membrane time constant τ.

Accordingly, the peak-to-peak MEP measurements V_{pp} are log-transformed through $y = \log(V_{\text{pp}})$, and the IO curve is modeled by the following sigmoid function

$$y = y^h + \frac{y^l - y^h}{1 + \Big(g_r r_p\Big)^s}. \tag{10}$$

where, y^l and y^h denote the lower and upper plateaus of the IO curve. The r_p value is small, thus the gain g_r is utilized to scale it up. The mid-point and slope of the IO curve are given by r_p and s.

The sigmoid model (10) is parameterized in the standard format, y versus V_C, as

$$y = \theta_2 + \frac{\theta_1 - \theta_2}{1 + \Big(\frac{V_C}{\theta_3}\Big)^{\theta_4}}, \tag{11}$$

where,

$$\boldsymbol{\theta} = [\ \theta_1 \quad \theta_2 \quad \theta_3 \quad \theta_4\ ] = [\ y^l \quad y^h \quad \tfrac{V_C}{g_r r_p} \quad s\ ]. \tag{12}$$

This is an integrated model of the neural membrane time constant and IO curve for cTMS, as τ appears in r_p and consequently θ_3. Figure 3 illustrates this integrated model structure for a cTMS pulse w to MEP y in a block diagram.

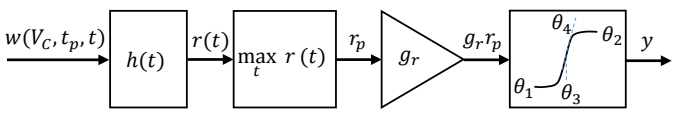

Figure 3: The functional block diagram of the integrated model of the neural membrane time constant and input–output curve from the cTMS pulse w to MEP y.

3. The Proposed Sequential Parameter Estimation Methods

3.1. Problem statement

The problem in this paper is to estimate the neural membrane time constant τ and the IO curve parameters θ_i, $i = 1, \ldots, 4$ in TMS.

In this section, two sequential parameter estimation (SPE) methods are proposed based on uniform and optimal sampling principles.

3.2. Outline of overall procedure

SPE starts with sampling from the baseline, administering three initial random pulses, measuring the corresponding MEPs, and computing the initial estimate of the IO curve parameters and time constant. The next TMS pulses are then chosen based on the uniform or optimal sampling methods. After the administration of each pulse, the corresponding MEP is measured, and the estimation of the IO curve and time constant is updated. The process continues until a stopping rule is satisfied or the maximum number of pulses is reached. Thus, the SPE method consists of four stages: initialization, selection of next TMS pulse, estimation update, and checking the stopping rule.

Notably, the entire estimation processes is a fully automatic online closed-loop procedure. It comprises the computation of the next TMS pulse with its specific parameters needed to extract most information in the next step via administration of the pulse to the EMG recording of the MEP response to the pulse and data analysis.

3.3. Initialization

In the initialization stage, the baseline data

$$\mathcal{D}_b = \{(0, y_{b_1}),\ (0, y_{b_2}),\ \ldots, (0, y_{n_b})\} \tag{13}$$

is collected. The baseline data is the EMG data in the absence of TMS pulse $V_C = 0$. In (13), n_b denotes the number of samples taken from the baseline. Then, three random TMS pulses with pulse strengths V_{C_1}, V_{C_2}, and V_{C_3} are administered and the corresponding MEPs y_1, y_2, and y_3 are measured. An initial estimate of the IO curve and time constant parameters is obtained by fitting the model (11) to the data set of

$$\mathcal{D}_{N_0=n_b+3} = \mathcal{D}_b \cup \{(V_{C_1}, y_1),\ (V_{C_2}, y_2),\ (V_{C_3}, y_3)\}. \tag{14}$$

The estimates of the IO curve parameters and time constant after the administration of the n-th stimulus V_{C_n} are named $\hat{\tau}_n$ and $\hat{\boldsymbol{\theta}}_n = [\theta_{i,n}]$, $i = 1, \ldots, 4$. At the end of the initialization stage, the procedure obtained $\hat{\tau}_3$ and $\hat{\boldsymbol{\theta}}_3 = [\theta_{i,3}]$, $i = 1, \ldots, 4$.

3.4. Selection of the next TMS pulse

In the next stage, the next TMS pulse is chosen by uniform or optimal sampling. In uniform sampling, the TMS stimuli are uniformly distributed between $V_C(\min)$ and $V_C(\max)$ and could be administered randomly or in an order, e.g., from weak to strong stimuli. However, studies show hysteresis due to strong correlation between subsequent responses, when pulses are administrated in an order [50, 51].

In the optimal sampling method, $V_{C_{n+1}}$ is determined by solving the optimization problem

$$\begin{aligned} \underset{V_{Cn+1}}{\text{minimize}} \quad & -\det\Big(\tilde{\mathbf{F}}_{n+1}(V_{C_{n+1}}, \hat{\tilde{\boldsymbol{\theta}}}_n)\Big) \\ \text{subject to} \quad & V_C(\min) \le V_{C_{n+1}} \le V_C(\max) \\ \text{for} \quad & 3 \le n \end{aligned} \tag{15}$$

where,

$$\begin{aligned} &\hat{\tilde{\boldsymbol{\theta}}}_n = [\hat{\theta}_{2,n}\ \hat{\theta}_{3,n}\ \hat{\theta}_{4,n}], \\ &\tilde{\mathbf{F}}_{n+1}(V_{C_{n+1}}, \hat{\tilde{\boldsymbol{\theta}}}_n) = \tilde{\mathbf{F}}_n(\mathbf{V}_{\mathbf{C}_n}, \hat{\tilde{\boldsymbol{\theta}}}_n) + \delta\tilde{\mathbf{F}}_{n+1}(V_{C_{n+1}}, \hat{\tilde{\boldsymbol{\theta}}}_n), \\ &\text{and } \mathbf{V}_{\mathbf{C}_n} = [\ V_{C_1} \quad V_{C_2} \quad \ldots \quad V_{C_n}\ ], \end{aligned}$$

following a fundamental concept suggested previously [33]. The matrices $\tilde{\mathbf{F}}_n$ and $\delta\tilde{\mathbf{F}}_{n+1}$ are given in Appendix B.

3.5. Estimation update

After each pulse V_{C_n}, $n > 3$, the corresponding MEP y_n is measured, and the data set is updated per

$$\mathcal{D}_{N=n_b+n} = \mathcal{D}_b \cup \{(V_{C_1}, y_1),\ (V_{C_2}, y_2), \ldots,\ (V_{C_n}, y_n)\}. \tag{16}$$

The estimation of $\hat{\boldsymbol{\theta}}_n = [\hat{\theta}_{i,n}]$, $i = 1, \ldots, 4$ is then updated by fitting the curve of (11) to the data set of $\mathcal{D}_{N=n_b+n}$. In order to mitigate the otherwise skewed variability, the curve fitting is performed on the logarithmic scale [25, 24].

After obtaining $\hat{\theta}_{3,n}$, the estimation of $\hat{\tau}_n$, $n > 3$ is obtained by solving

$$\begin{aligned} \hat{\theta}_{3,n} - \frac{\alpha\hat{\tau}_n^2 - 2\sigma\hat{\tau}_n + 1}{g_r k_1}\Big(& -\omega e^{-t^*/\hat{\tau}_n} \\ & + \Big((\alpha\hat{\tau}_n - \sigma)\sin\omega t^* + \omega\cos\omega t^*\Big)e^{-\sigma t^*}\Big)^{-1} = 0, \end{aligned} \tag{17}$$

where, t^* is the time at which the linearized neural membrane depolarization reaches its maximum as described in Section 2.2.

A previously developed bad-fit detection and removal technique is employed as described in the literature to improve curve fitting and solving the nonlinear equation (17) [33, 34].

3.6. Termination of checking the stopping rule

The process continues until a stopping rule is satisfied or the maximum number of pulses is reached. The SPE is terminated when the following constraint is satisfied for T successive times

$$\left|\frac{\hat{\theta}_{l,n} - \hat{\theta}_{l,n-1}}{\hat{\theta}_{l,n-1}}\right| < \epsilon_\theta, \text{ for } l = 1, \ldots, 4, \tag{18}$$

$$\left|\frac{\hat{\tau}_n - \hat{\tau}_{n-1}}{\hat{\tau}_{n-1}}\right| < \epsilon_\tau \tag{19}$$

where, ϵ_θ and ϵ_τ denote the estimation tolerance of $\boldsymbol{\theta}$ and τ, respectively. To reduce premature terminations, $T > 1$ is strongly suggested as discussed in the literature, [33].

4. Identifiability Analysis

After administering the n-th cTMS pulse ($n \geq 3$), $\hat{\theta}_{3,n}$ is obtained through curve regression. In order to continue the SPE method, the nonlinear equation (17) with two parameters $\hat{\boldsymbol{\theta}}_n$ and $\hat{\tau}_n$ must be solvable. Thus, the identifiability of the IO curve and membrane time constant depends on the solution of (17).

If t^* is known, $\hat{\tau}_n$ will be the only unknown parameter in (17), which can be found by using numerical methods. Based on the discussions in Section 2.2, t^* is known only if t_p is less than the critical pulse width t_p^*. Thus, the short pulse width is recommended from the identifiability perspective. In this case, r_p occurs at the end of the pulse width, $t^* = t_p$, the nonlinear equation (17) is solvable, and the parameters $\hat{\boldsymbol{\theta}}_n$ and $\hat{\tau}_n$ are identifiable.

Remaining is the solution of the nonlinear equation (17) with the known t^* and unknown $\hat{\theta}_{3,n}$. Fig. 4 displays $\hat{\theta}_{3,n}$ versus $\hat{\tau}_n$ for different t^*s. For $t^* = 30\ \mu s$, a unique $\hat{\tau}_n$ is obtained for almost all $\hat{\theta}_{3,n}$s. For $t^* = 60\ \mu s$, two $\hat{\tau}_n$s are obtained for $\hat{\theta}_{3,n} \leq 0.16$, and there will be a unique solution for $\hat{\theta}_{3,n} > 0.16$. By increasing the t^* value, the region that results in two $\hat{\tau}_n$s increases. The acceptable time constant is obtained based on the neurophysiological or microanatomical characteristics of the neural membrane.

5. Simulation Results

Consider 10,000 stimulus-response pairs, shown by '×', in Fig.5-a, generated by using parts of a realistic MEP model and combining it with the same integration of the activation dynamics as in Eq. (11) and Fig. 3 with the following randomly chosen neural time constant and IO curve parameters [52]

$$\tau^{\text{true}} = 201.93\ \mu s,$$
$$\boldsymbol{\theta}^{\text{true}} = [\ -6.05 \quad -2.34 \quad 0.41 \quad 18.48\ ].$$

From Fig. 2, the critical pulse width for $\tau^{\text{true}} = 201.93$ is $t_p^* = 123.9\ \mu s$. Thus, the integrated model is identifiable

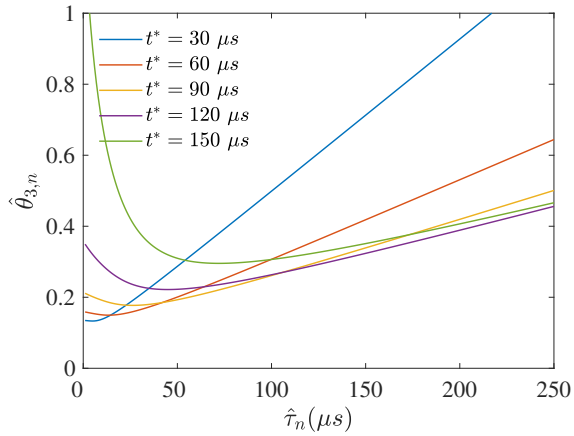

Figure 4: Identifiability of $\hat{\tau}_n$.

for pulse widths less than 123.9 μs. The pulse width is randomly fixed at $t_p = 100\ \mu s$. $t_p = 100\ \mu s < t_p^* = 123.9\ \mu s$, thus, $t^* = t_p = 100\ \mu s$. The gain g_r is set to 40.

The random noise along the x and y axes are generated by zero-mean normal functions with standard deviation of 0.05 and 0.1, respectively. The y axis denotes the MEP's peak-to-peak value used in the simulation. The solid line in Fig. 5-a shows the true IO curve in the absence of x and y variabilities.

The problem in this section is to estimate the neural time constant and IO curve parameters by using the uniformly sampling and optimal IO curve SPE methods. The stopping rule is set up with $T = 5$, i.e., five times consecutive satisfaction of the convergence criteria in (18) and (19) with $\epsilon_\theta = \epsilon_\tau = 0.01$. The maximum number of TMS pulses is set to $N_{\max} = 150$. Fifty samples are taken from the baseline for both methods.

The simulation is run in Matlab. The estimation update runs a trust-region regression algorithm with lower and upper limits on the parameter vector per

$$\boldsymbol{\theta}_{\min} = [\ -7 \quad -3 \quad 0 \quad 1\ ],$$
$$\boldsymbol{\theta}_{\max} = [\ -5 \quad -1 \quad 1 \quad 100\ ].$$

The FIM optimization of Eq. (15) and the estimation of Eq. (17) are solved by using 'fmincon', the 'interior-point' algorithm, and the 'GlobalSearch' method.

The FIM SPE method satisfied the stopping rule at $n = n_f = 62$, while the uniform sampling SPE did not fulfill the stopping rule at all. Figures 5-b and c show the acquired samples and estimated IO curves by the FIM SPE and the uniformly sampling method at $n_f = 62$ and $N_{max} = 150$, respectively. As discussed in [33], it is seen that the FIM SPE method administers stimuli, mainly from three regions, which contain the maximum information of the IO curve. These regions include two sectors from the slope area and one sector at around $x_{\max} = 1$. In contrast, the uniform sampling administers TMS stimuli across the entire range of $x = 0$ to $x = 1$. Figure 6 displays the estimates of θ_i, $i = 1, \ldots, 4$ with increasing pulse number.

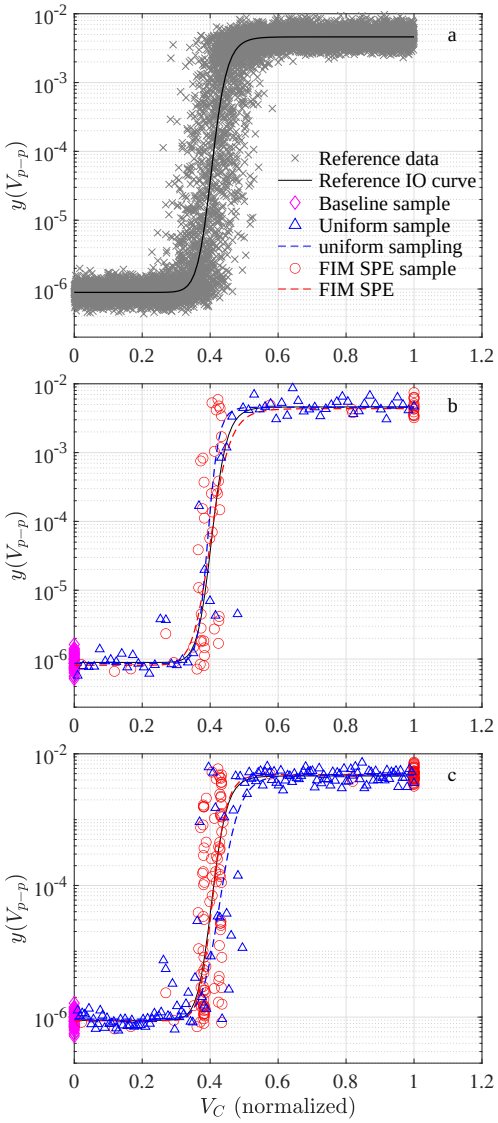

Figure 5: Sample simulation run: (a) reference data and IO curve, and estimation by using the FIM and uniform sampling methods at $n = n_f = 62$ (b) and at $n = n_{\max} = 150$ (c).

Figure 7, in turn, provides the corresponding τ.

All results confirm that the TMS neural time constant, IO curve, and its parameters are satisfactorily estimated using the proposed SPE methods based on the uniformly sampling and the FIM-based sampling principles. It should be noted that previous comparisons clarifying the differences between the uniform and FIM SPE of the IO curve are still valid here [33]. With reference to the results of 10 177 simulation runs in [33], the low and high plateaus and mid-point (θ_1, θ_2, and θ_3, respectively) are estimated with a median relative error of less than 2% for $T = 5$. The slope θ_4 is estimated with the median relative error of less than 20% for $T = 5$. Note that the neural time constant τ relates only to θ_3 through (12). Thus, the estimation error of τ is proportional to the estimation error of θ_3.

6. Conclusions and future works

This paper describes a novel formalism for sequential parameter estimation (SPE) of the neural time constant through the input–output (IO) curve and its parameters in transcranial magnetic stimulation (TMS). Analytical calculation of the depolarization factor was discussed. An integrated model was developed based on the depolarization factor, relating the neural recruitment curve and time constant. The identifiability of the proposed integrated model was analyzed. The formalism was linked with uniform and FIM sampling principles. The results demonstrate estimation of the neural time constant through the input–output curve and its parameters in the presence of x and y variability. Without loss of generality, this paper focused on a specific case of cTMS pulses. The method is directly applicable to other cTMS pulse shapes with no new point of principals.

7. Appendix A

The state-space representation of the neural membrane dynamic $h(t)$ is given by

$$h(t) : \begin{cases} \dot{z}(t) = \bar{A}z(t) + \bar{B}w(t) \\ r(t) = \bar{C}z(t). \end{cases}$$

where z and r are the membrane state and response with

$$\bar{A} = -1/\tau,\ \bar{B} = 1/\tau,\ \bar{C} = g_c.$$

Given the system matrices $\bar{A}$, $\bar{B}$, and $\bar{C}$, the membrane response $r(t)$ is computed by using

$$\begin{aligned} r(t) &= \bar{C}e^{\bar{A}(t-t_0)}z(t_0) + \bar{C}\int_{t_0}^{t} e^{\bar{A}(t-\xi)}\bar{B}w(\xi)d\xi \\ &= r(t_0)e^{\bar{A}(t-t_0)} + \bar{C}\int_{t_0}^{t} e^{\bar{A}(t-\xi)}\bar{B}w(\xi)d\xi, \end{aligned}$$

where t_0 is the initial time [53].

Within the first phase of $w(t)$, i.e., $t \le t_p$, $t_0 = 0$, $r(0) = 0$, the membrane response is computed as

$$\begin{aligned} r(t) &= g_c\int_0^t e^{-(t-\xi)/\tau}\frac{1}{\tau}\frac{\delta V_C}{L}(\cos\omega\xi - \frac{\sigma}{\omega}\sin\omega\xi)e^{-\sigma\xi}d\xi \\ &= \frac{g_c\delta V_C}{L\tau}e^{-t/\tau}\int_0^t(\cos\omega\xi - \frac{\sigma}{\omega}\sin\omega\xi)e^{(1/\tau-\sigma)\xi}d\xi. \end{aligned}$$

By defining $a = 1/\tau - \sigma$, the integration by parts results in

$$\begin{aligned} r(t) &= \frac{g_c\delta V_C}{L\tau\omega(\omega^2+a^2)}e^{-t/\tau}\times \\ &\quad \left((\omega^2 - a\sigma)\sin\omega\xi + \frac{\omega}{\tau}\cos\omega\xi\right)e^{a\xi}\Big|_{\xi=0}^{\xi=t} \\ &= \frac{g_c\delta V_C}{L\tau\omega(\omega^2+a^2)}e^{-t/\tau}\times \\ &\quad \left[\left((\omega^2 - a\sigma)\sin\omega t + \frac{\omega}{\tau}\cos\omega t\right)e^{at} - \frac{\omega}{\tau}\right]. \end{aligned}$$

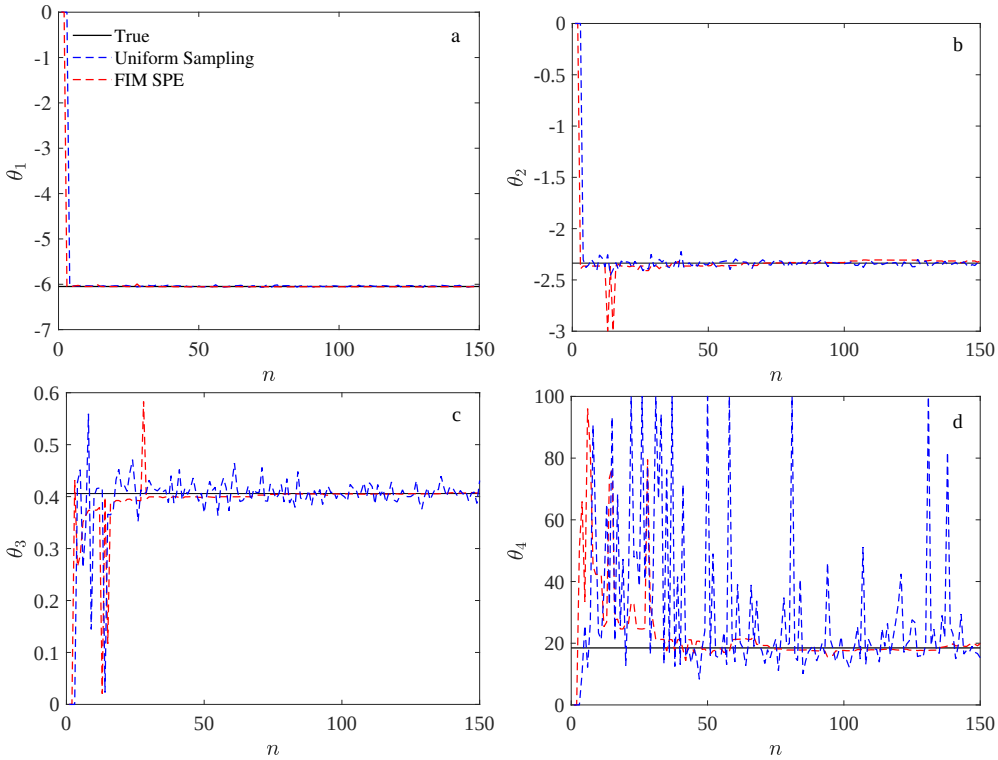

Figure 6: Estimated IO curve parameters: (a) lower plateau, (b) upper plateau, (c) mid-point, and (d) slope.

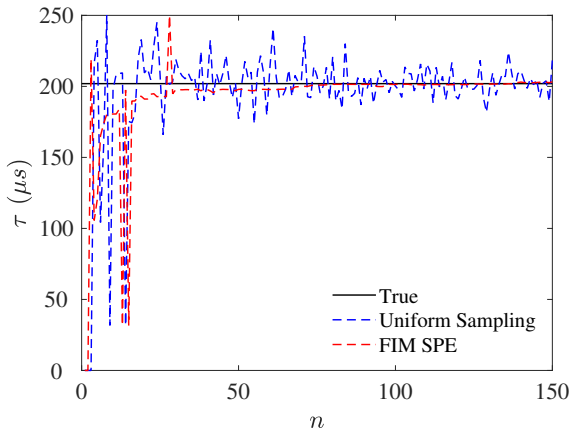

Figure 7: Estimated neural time constant.

Defining $k_1 = g_c\delta/(L\omega)$ and $\alpha = \omega^2 + \sigma^2$ results in the part of Eq. (8) for $t \leq t_p$.

Within the second phase of $w(t)$, i.e., $t > t_p$, $t_0 = t_p^+$, where t_p^+ denotes a time slightly after t_p. By using the approximation $Cz(t_0) = g_c z(t_p^+) = r(t_p^+) \approx r(t_p)$, the membrane response is computed as follows,

$$
\begin{aligned}
r(t) &= e^{-(t-t_p)/\tau} r(t_p) + \\
& g_c \int_{t_p^+}^{t} e^{-(t-\xi)/\tau} \frac{-\delta V_C (R+r)\sin\omega t_p}{\tau\omega L^2} e^{-\frac{(\xi-t_p)(R+r)}{L} - \sigma t_p} d\xi \\
&= e^{-(t-t_p)/\tau} r(t_p) + \\
& \frac{-g_c\delta V_C (R+r)\sin\omega t_p}{\tau\omega L^2} e^{-t/\tau} e^{t_p(\frac{R+r}{L}-\sigma)} \int_{t_p^+}^{t} e^{(\frac{1}{\tau}-\frac{R+r}{L})\xi} d\xi \\
&= e^{-(t-t_p)/\tau} r(t_p) + \frac{-g_c\delta V_C (R+r)\sin\omega t_p}{\tau\omega L^2 (1/\tau - (R+r)/L)} \times \\
& e^{-t/\tau} e^{t_p(\frac{R+r}{L}-\sigma)} e^{(\frac{1}{\tau}-\frac{R+r}{L})\xi} \Big|_{\xi=t_p^+}^{\xi=t}
\end{aligned}
$$

With the approximation $t_p^+ \approx t_p$,

$$
\begin{aligned}
r(t) = e^{-(t-t_p)/\tau} r(t_p) + \frac{-g_c\delta V_C (R+r)\sin\omega t_p}{\tau\omega L^2 (1/\tau - (R+r)/L)} \times \\
\left(e^{-(t-t_p)(R+r)/L} - e^{-(t-t_p)/\tau} \right) e^{-\sigma t_p}
\end{aligned}
$$

Defining $k_2 = \frac{k_1 (R+r)\sin\omega t_p}{\tau L(1/\tau - (R+r)/L)}$ leads to the part of Eq. (8) for $t > t_p$.

8. Appendix B

The matrices in the FIM optimization problem per Eq. (15) are computed as follows. The matrix $\mathbf{F}_n(\mathbf{V}_{\mathbf{C}_n}, \hat{\hat{\boldsymbol{\theta}}}_n)$,

$n \geq 3$ is given by

$$\mathbf{F}_n(\mathbf{V}_{\mathbf{C}_n}, \tilde{\hat{\boldsymbol{\theta}}}_n) = \Big[f_{rq}\Big]_n \text{ for } r, q = 1, \ldots, 3,$$

where

$$f_{rq} = \mathrm{dot}(\mathbf{f}_r, \mathbf{f}_q),$$

$$\mathbf{D}(\mathbf{V}_{\mathbf{C}_n}, \hat{\boldsymbol{\theta}}_n) = 1 + \left(\frac{\mathbf{V}_{\mathbf{C}_n}}{\hat{\theta}_{3,n}}\right)^{\hat{\theta}_{4,n}},$$

$$\mathbf{f}_1 = 1 - \frac{1}{\mathbf{D}(\mathbf{V}_{\mathbf{C}_n}, \hat{\boldsymbol{\theta}}_n)},$$

$$\mathbf{f}_2 = \frac{(\hat{\theta}_{1,n} - \hat{\theta}_{2,n})\hat{\theta}_{4,n}\hat{\theta}_{3,n}^{-\hat{\theta}_{4,n}-1}\mathbf{V}_{\mathbf{C}_n}^{\hat{\theta}_{4,n}}}{\Big(\mathbf{D}(\mathbf{V}_{\mathbf{C}_n}, \hat{\boldsymbol{\theta}}_n)\Big)^2},$$

$$\mathbf{f}_3 = -\frac{(\hat{\theta}_{1,n} - \hat{\theta}_{2,n})\hat{\theta}_{3,n}^{-\hat{\theta}_{4,n}}\mathbf{V}_{\mathbf{C}_n}^{\hat{\theta}_{4,n}} \ln\Big(\frac{\mathbf{V}_{\mathbf{C}_n}}{\hat{\theta}_{3,n}}\Big)}{\Big(\mathbf{D}(\mathbf{V}_{\mathbf{C}_n}, \hat{\boldsymbol{\theta}}_n)\Big)^2}.$$

The bilinear form $\mathrm{dot}(\mathbf{f}_r, \mathbf{f}_q)$ returns the scalar product of the vectors $\mathbf{f}_r$ and $\mathbf{f}_q$.

The matrix $\delta\tilde{\mathbf{F}}_{n+1}(V_{C_{n+1}}, \hat{\tilde{\boldsymbol{\theta}}}_n)$, $n \geq 3$ is computed per

$$\delta\tilde{\mathbf{F}}_{n+1}(V_{C_{n+1}}, \hat{\tilde{\boldsymbol{\theta}}}_n) = \Big[\delta f_{rq}\Big]_{n+1} \text{ for } r, q = 1, \ldots, 3$$

where

$$\delta f_{rq} = \mathrm{dot}(f_r, f_q),$$

$$D(V_{C_{n+1}}, \hat{\boldsymbol{\theta}}_n) = 1 + \Big(\frac{V_{C_{n+1}}}{\hat{\theta}_{3,n}}\Big)^{\hat{\theta}_{4,n}},$$

$$f_1 = 1 - \frac{1}{D(V_{C_{n+1}}, \hat{\boldsymbol{\theta}}_n)},$$

$$f_2 = \frac{(\hat{\theta}_{1,n} - \hat{\theta}_{2,n})\hat{\theta}_{4,n}\hat{\theta}_{3,n}^{-\hat{\theta}_{4,n}-1}V_{C_{n+1}}^{\hat{\theta}_{4,n}}}{\Big(D(V_{C_{n+1}}, \hat{\boldsymbol{\theta}}_n)\Big)^2},$$

$$f_3 = -\frac{(\hat{\theta}_{1,n} - \hat{\theta}_{2,n})\hat{\theta}_{3,n}^{-\hat{\theta}_{4,n}}V_{C_{n+1}}^{\hat{\theta}_{4,n}} \ln\Big(\frac{V_{C_{n+1}}}{\hat{\theta}_{3,n}}\Big)}{\Big(D(V_{C_{n+1}}, \hat{\boldsymbol{\theta}}_n)\Big)^2}.$$

References

[1] Polson MJ, Barker AT, Freeston IL. Stimulation of nerve trunks with time-varying magnetic fields. Medical & biological engineering & computing 1982; 20(2):243–244.

[2] Barker AT, Jalinous R, Freeston IL. Non-invasive magnetic stimulation of human motor cortex. The Lancet 1985; 325(8437):1106–1107.

[3] Caramia MD, Pardal AM, Zarola F, Rossini PM. Electric vs magnetic trans-cranial stimulation of the brain in healthy humans: a comparative study of central motor tracts 'conductivity'and 'excitability'. Brain research 1989; 479(1):98–104.

[4] Gomez LJ, Goetz SM, Peterchev AV. Design of transcranial magnetic stimulation coils with optimal trade-off between depth, focality, and energy. Journal of Neural Engineering 2018; 15:046033.

[5] Halawa I, Shirota Y, Neef A, Sommer M, Paulus W. Neuronal tuning: Selective targeting of neuronal populations via manipulation of pulse width and directionality. Brain Stimulation 2019; 12(5):1244–1252.

[6] Goetz SM, Luber B, Lisanby SH, Murphy DLK, Kozyrkov AC, Grill WM, Peterchev AV. Enhancement of Neuromodulation with Novel Pulse Shapes Generated by Controllable Pulse Parameter Transcranial Magnetic Stimulation. Brain Stimulation 2016; 9:39–47.

[7] Rattay F, Paredes LP, Leao RN. Strength–duration relationship for intra- versus extracellular stimulation with microelectrodes. Neuroscience 2012; 214:1–13.

[8] Peterchev AV, Jalinous R, Lisanby SH. A Transcranial Magnetic Stimulator Inducing Near-Rectangular Pulses With Controllable Pulse Width (cTMS). IEEE Trans Biomed Eng 2008; 55(1):257–66.

[9] Isokawa M. Membrane time constant as a tool to assess cell degeneration. Brain Res Brain Res Protoc. 1997 May; 1(2):114–6.

[10] Geddes LA. Accuracy limitations of chronaxie values. IEEE Trans Biomed Eng. 2004; 51:176–181.

[11] Boinagrov D, Loudin J, Palanker D. Strength–duration relationship for extracellular neural stimulation: numerical and analytical models. J Neurophysiol. 2010; 104:2236–2248.

[12] Mogyoros I, Kiernan MC, Burke D. Strength-duration properties of human peripheral nerve. Brain 1996; 119 (Pt 2):439–47.

[13] Lugg A, Schindle M, Sivak A, Tankisi H, Jones KE. Nerve excitability as a biomarker for amyotrophic lateral sclerosis: a systematic review and meta-analysis. medRxiv 2022; doi: https://doi.org/10.1101/2022.02.11.22270866

[14] Farrar MA, Vucic S, Lin CS, Park SB, Johnston HM, du Sart D, et al. Dysfunction of axonal membrane conductances in adolescents and young adults with spinal muscular atrophy. Brain. 2011; 134:3185–3197.

[15] Moldovan M, Alvarez S, Pinchenko V, Marklund S, Graffmo KS, Krarup C. Nerve excitability changes related to axonal degeneration in amyotrophic lateral sclerosis: Insights from the transgenic SOD1(G127X) mouse model. Exp Neurol. 2012; 233:408–420.

[16] Lin CS, Krishnan AV, Park SB, Kiernan MC. Modulatory effects on axonal function after intravenous immunoglobulin therapy in chronic inflammatory demyelinating polyneuropathy. Arch Neurol. 2011; 68:862–869.

[17] Yerdelen D, Koc F, Uysal H. Strength–duration properties of sensory and motor axons in alcoholic polyneuropathy. Neurological Research 2008; 30(7): 746–750.

[18] Goetz SM, Kammer T. Neuronavigation. In The Oxford Handbook of Transcranial Stimulation, Second edition, Oxford 2022.

[19] Klomjai W, Katz R, Lackmy-Vallée. Basic principles of transcranial magnetic stimulation (TMS) and repetitive TMS (rTMS). Annals of Physical and Rehabilitation Medicine 2015; 58(4):208–213.

[20] Westin GG, Bassi BD, Lisanby SH, Luber B. Determination of motor threshold using visual observation overestimates transcranial magnetic stimulation dosage: safety implications. Clinical Neurophysiology 2014; 125(1):142–147.

[21] Li Z, Peterchev AV, Rothwell JC, Goetz SM. Detection of Motor-Evoked Potentials Below the Noise Floor: Rethinking the Motor Threshold. bioRxiv 2021.12.10.472126.

[22] Goetz SM, Li Z, Peterchev AV. Noninvasive detection of motor-evoked potentials in response to brain stimulation below the noise floor—how weak can a stimulus be and still stimulate. Proc IEEE Eng Med Biol Soc (EMBC) 2018; 40:2687–2690.

[23] Geddes LA. Optimal stimulus duration for extracranial cortical stimulation. Neurosurgery 1987; 20(1):94–99.

[24] Peterchev AV, Goetz SM, Westin GG, Luber B, Lisanby SH. Pulse width dependence of motor threshold and input–output curve characterized with controllable pulse parameter transcranial magnetic stimulation. Clinical Neurophysiology 2013; 124:1364–1372.

[25] D'Ostilio K, Goetz SM, Hannah R, Ciocca M, Chieffo R, Chen

J-C A, Peterchev AV, Rothwell JC. Effect of coil orientation on strength–duration time constant and I-wave activation with controllable pulse parameter transcranial magnetic stimulation. Clinical Neurophysiology 2016; 127:675–683.

[26] Nowak LG, Bullier J. Axons, but not cell bodies, are activated by electrical stimulation in cortical gray matter. I: Evidence from chronaxie measurements. Exp Brain Res. 1998; 118:477–488.

[27] Karabanov A, Thielscher A, Siebner HR. Transcranial brain stimulation: Closing the loop between brain and stimulation. Curr Opin Neurol 2016;29(4):397–404.

[28] Tervo AE, Nieminen JO, Lioumis P, Metsomaa J, Souza VH, Sinisalo H, Stenroos M, Sarvas J, Ilmoniemia RJ. Closed-loop optimization of transcranial magnetic stimulation with electroencephalography feedback, Brain Stimulation 2021; 14:P1674.

[29] Bergmann TO, Mölle M, Schmidt MA, Lindner C, Marshall L, Born J, Siebner HR. EEG-guided transcranial magnetic stimulation reveals rapid shifts in motor cortical excitability during the human sleep slow oscillation. Journal of Neuroscience 2012; 32(1):243–53.

[30] Zrenner C, Desideri D, Belardinelli P, Ziemann U. Real-time EEG-defined excitability states determine efficacy of TMS-induced plasticity in human motor cortex, Brain Stimulation 2018; 11(2):374–389.

[31] Ding Z, Ouyang G, Chen H, Li X. Closed-loop transcranial magnetic stimulation of real-time EEG based on the AR mode method. Biomed. Phys. Eng. Express 2020; 6:035010.

[32] Pankka H, Roine T, Lehtinen J, Ilmoniemi, RJ. Improving closed-loop TMS timing using the Wavenet model. Brain Stimulation 2021; 14(6):P1636–1637.

[33] Alavi SMM, Goetz SM, Peterchev AV. Optimal estimation of neural recruitment curves using Fisher information: application to transcranial magnetic stimulation. IEEE Transactions on Neural Systems and Rehabilitation Engineering 2019; 27:1320–1330.

[34] Alavi SMM, Goetz SM, Saif M. input–output Slope Curve Estimation in Neural Stimulation Based on Optimal Sampling Principles. Journal of Neural Engineering 2021; 18:046071.

[35] Kemlin C, Moulton E, Leder S, Houot M, Meunier S, Rosso C, Lamy J-C. Redundancy Among Parameters Describing the input–output Relation of Motor Evoked Potentials in Healthy Subjects and Stroke Patients. Frontiers in Neurology 2019; 10:Article 535.

[36] van de Ruit M, Pearson T, Grey MJ. Novel tools for rapid online data acquisition of the TMS stimulus-response curve. Brain Stimulation 2019; 1:192–194.

[37] Giridharan SR, Gupta D, Pal A, Mishra AM, Hill NJ, Carmel JB. Motometrics: A Toolbox for Annotation and Efficient Analysis of Motor Evoked Potentials. Frontiers in Neuroinformatics 2019; 13:Article 8.

[38] Goetz SM, Deng ZD. The Development and Modelling of Devices and Paradigms for Transcranial Magnetic Stimulation. International Review of Psychiatry 2017; 29(2):115–145.

[39] Goetz S, Weyh T, Herzog HG. Temporal Analysis of Magnetic Nerve Stimulation. Journal of Electrical and Computer Engineering 2009; 3(10):1798–1801.

[40] Goetz SM, Weyh T, Afinowi IAA, Herzog HG. Coil Design for Neuromuscular Magnetic Stimulation Based on a Detailed 3-D Thigh Model. IEEE Transactions on Magnetics 2014; 50(6):1–10.

[41] Corthout E, Barker AT, Cowey A. Transcranial magnetic stimulation. Which part of the current waveform causes the stimulation? Exp Brain Res 2001; 141:128-–32.

[42] Goetz SM, Pfaeffl M, Huber J, Singer M, Marquardt R, Weyh T. Circuit topology and control principle for a first magnetic stimulator with fully controllable waveform. Proc IEEE Eng Med Biol Soc (EMBC) 2012; 34:4700–4703.

[43] Li Z, Zhang J, Peterchev AV, Goetz SM. Modular Pulse Synthesizer for Transcranial Magnetic Stimulation with Flexible User-Defined Pulse Shaping and Rapidly Changing Pulses in Sequences. arXiv 2022; 2202.06530.

[44] Zeng Z, Koponen LM, Hamdan R, Li Z, Goetz SM, Peterchev AV. Modular multilevel TMS device with wide output range and ultrabrief pulse capability for sound reduction. Journal of Neural Engineering 2022; 19(2):026008.

[45] Barker AT, Garnham CW, Freeston IL. Magnetic nerve stimulation: the effect of waveform on efficiency, determination of neural membrane time constants and the measurement of stimulator output. Electroencephalogr Clin Neurophysiol Suppl 1991; 43:227–37.

[46] Goetz SM, Peterchev AV. A model of variability in brain stimulation evoked responses. Proceedings of the IEEE Engineering in Medical and Biology Society (EMBC) 2012; 34:6434–6437.

[47] Goetz SM, Howell B, Wang B, Li Z, Sommer MA, Peterchev AV, Grill WM. Isolating two sources of variability of subcortical stimulation to quantify fluctuations of corticospinal tract excitability. Clinical Neurophysiology 2022. doi: 10.1016/j.clinph.2022.02.009

[48] Nielsen JF. Logarithmic distribution of amplitudes of compound muscle action potentials evoked by transcranial magnetic stimulation. Journal of Clinical Neurophysiology 1996; 13(5):423–434.

[49] Goetz SM, Luber B, Lisanby SH, Peterchev AV. A Novel Model Incorporating Two Variability Sources for Describing Motor Evoked Potentials. Brain Stimulation 2014; 7:541–552.

[50] Möller C, Arai N, Lucke J, Ziemann U. Hysteresis Effects of Cortico-Spinal Excitability during Transcranial Magnetic Stimulation. Front. Comput. Neurosci. Conference Abstract: Bernstein Conference on Computational Neuroscience 2009; doi: 10.3389/conf.neuro.10.2009.14.124.

[51] Vaseghi B, Zoghi M, Jaberzadeh S. Inter-pulse Interval Affects the Size of Single-pulse TMS-inducedMotor Evoked Potentials: A Reliability Study. Basic and Clinical Neuroscience 2015; 6(1):44 – 51.

[52] Goetz SM, Alavi SMM, Deng ZD, Peterchev AV. Statistical Model of Motor-Evoked Potentials. IEEE Transactions on Neural Systems and Rehabilitation Engineering 2019; 27(8):1539-1545.

[53] Brogen, W.L., *Modern Control Theory*, 3rd Ed, Prentice Hall, 1991.